Review and Evaluation of Models for Self-Pressurizing Propellant Tank Dynamics

Jonah E. Zimmerman*, Benjamin S. Waxman†, and Brian J. Cantwell‡
Stanford University, Stanford, CA, 94305, USA

Gregory G. Zilliac§
NASA Ames Research Center, Moffett Field, CA, 94035, USA

Nitrous oxide is a popular oxidizer choice for many in the hybrid rocket community due to its ease of handling, storability at room temperature, and high vapor pressure. This high vapor pressure can be used as the pressurant, making it what is referred to as a self-pressurizing propellant. Unfortunately no comprehensive models exist for the dynamics of a self-pressurizing propellant tank and thus the modeling of system performance of nitrous oxide hybrids is difficult. In this paper, three existing models (equilibrium, Zilliac & Karabeyoglu, Casalino & Pastrone) of the system are described, evaluated, and compared against a variety of experimental data. The Zilliac & Karabeyoglu model performs the best in 5 of the 6 test cases but is limited by its complexity and its requirement of an empirical factor that is system-dependent. The equilibrium model does not capture the initial transient behavior and often over-predicts the pressure but is the simplest model and requires properties at saturation only. The Casalino & Pastrone model is a compromise between the two but does not perform well here, possibly due to differences in sources for thermodynamic properties.

Nomenclature

β	Volumetric thermal expansion coefficient
Δh_{LV}	Enthalpy of vaporization
$\dot{m}$	Mass flow rate
$\dot{Q}$	Rate of heat transfer
$\dot{W}$	Rate of work transfer
κ	Parameter from Dyer flow model
$\mathfrak{M}$	Molecular mass
Nu	Nusselt number
μ	Dynamic viscosity
ρ	Density
A	Area
c	Specific heat capacity or convection constant
C_d	Discharge coefficient
c_P	Isobaric specific heat capacity
c_V	Isochoric specific heat capacity
E	Heat transfer empirical factor
G	Mass flux
g	Acceleration due to gravity
h	Specific enthalpy or heat transfer coefficient
k	Thermal conductivity
L	Length scale
P	Pressure
R	Universal gas constant
r	Radius
Ra	Rayleigh number
T	Temperature
t	Time
U	Internal energy
u	Specific internal energy
V	Volume
v	Speed
x	Fluid quality
Z	Gas compressibility factor
z	Vertical coordinate

Subscripts

*PhD Candidate, SPaSE Lab, Department of Aeronautics & Astronautics, AIAA Member (jonahz@stanford.edu).
†PhD Candidate, SPaSE Lab, Department of Aeronautics & Astronautics, AIAA Member (waxman@stanford.edu).
‡Professor, Department of Aeronautics & Astronautics, AIAA Fellow.
§Research Scientist, NASA Ames Research Center, AIAA Member.

1	Upstream of the injector
2	Downtream of the injector
HEM	Homogeneous equilibrium model
SPI	Single phase incompressible
surf	Saturated liquid layer surface
ave	Average
cond	Conduction or condensation
evap	Evaporation
exp	Value from experiment
i	Inner or initial
in	Into the node
lim	Limit
liq	Liquid
LRO	Liquid run out point
model	Value from model
nonsat	Non-saturation or not saturated
o	Outer
opt	Optimal
out	Out of the node
outlet	Flow out through the injector
sat	Saturation or saturated
spin	Spinodal
tank	Tank property
tot	Total
vap	Vapor
w	Wall property

I. Introduction

The oxidizer of choice for many hybrid rocket propulsion systems is nitrous oxide. Thermochemically its performance is similar to hydrogen peroxide or nitric acid, but in many ways it is operationally simpler to use. The primary reasons are that it is non-toxic, requires little or no thermal control, and is therefore relatively easy to handle. Additionally, nitrous oxide's vapor pressure at standard conditions is high enough that often an external pressurization system is unneeded.

In this configuration it is known as a self-pressurizating propellant and can be used to make a very simple propulsion system. This not only reduces overall complexity but also inert mass by eliminating pressurant tanks, regulators, and valves. A significant drawback to using nitrous oxide as a self-pressurizing propellant is that modeling the oxidizer is quite difficult. As a tank of self-pressurized nitrous oxide is drained heat and mass transfer occurs between the liquid and vapor phases in the form of diffusion, convection, boiling, condensation, and evaporation. If these are not all correctly accounted for the oxidizer flowrate cannot be accurately predicted. A pressure trace from a hybrid rocket motor test using nitrous oxide as a self-pressurizing propellant is shown in figure 1.

The primary features of figure 1 are typical of self-pressurizing propellant tank dynamics: a steep drop followed by a short increase, then a linear drop towards a sharp cusp. The cusp (at $t = 9s$ here) is the point when no liquid remains in the tank and only vapor flows out. Gas-only flow out of the tank can be an undesirable situation due to the hazards of nitrous oxide decomposition events[2] and therefore motor firings are often terminated when the liquid has been used up. In this paper, only the portion of a blow-down when liquid is exiting the tank will be evaluated.

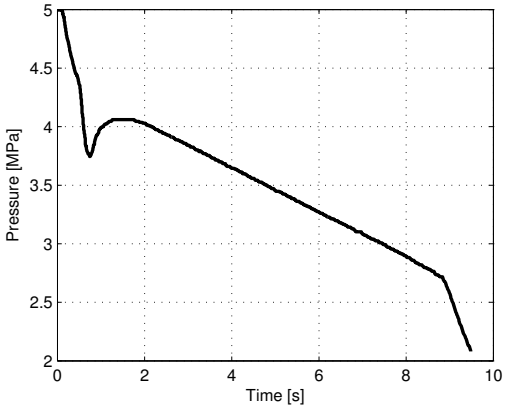

Figure 1. Pressure time history from a hybrid motor test firing, from Van Pelt et al[1]

Several groups have developed models for nitrous oxide tank dynamics. This includes Whitmore & Chandler,[3] Zilliac & Karabeyoglu,[4] and Casalino & Pastrone.[5] However, while these models have been used by these researchers to reproduce their own experimental results they use conflicting assumptions and it remains unclear which model (if any) is valid for a given system. This uncertainty stems from the fundamental lack of knowledge about what is going on inside a draining self-pressurized propellant tank.

To shed light on the mystery, experiments have been performed by the authors (Zimmerman et al[6,7]) with a transparent polycarbonate propellant tank that enables video measurements of the liquid and vapor as the tank is drained. These tests are ongoing, but to date they have identified significant boiling and condensation.

In this paper, three models will be evaluated: an equilibrium model, a non-equilibrium model similar to Zilliac & Karabeyoglu, and the non-equilibrium model of Casalino & Pastrone. The goal is to examine the

performance of each of these models by comparing to several sets of experimental data.

II. Common Model Features

These three models share many similar features. These will be discussed first, followed by a derivation of each model and a description of its main features. The common features between the models include some basic physical assumptions and mathematical forms, characterization of the flow out of the tank, heat transfer calculations, and numerical methods.

A. Fundamental Theory

The models all begin by dividing the tank into a small number of regions and representing each as a single node with averaged properties. Figure 2 shows the four nodes used by the models discussed in this paper: the liquid nitrous oxide, the vapor nitrous oxide, the portion of the tank wall in contact with the liquid, and the portion of the tank wall in contact with the vapor.

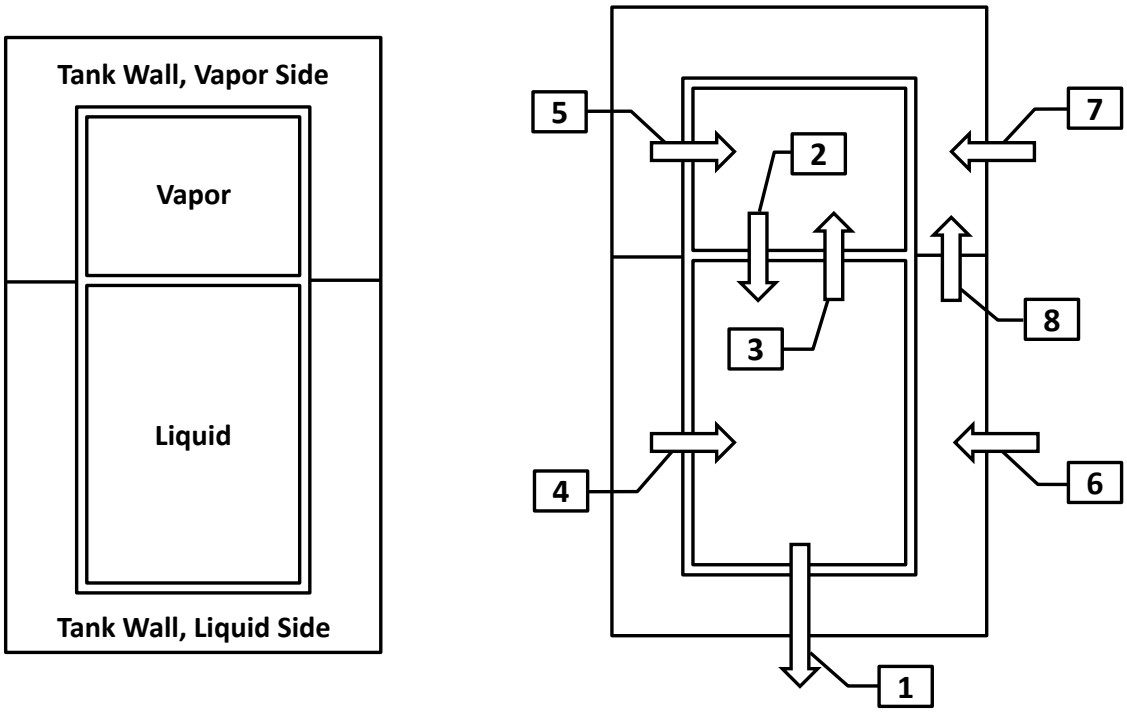

(a) Nodes (b) Heat and Mass Transfer

Figure 2. Diagrams showing the nodes and the heat and mass transfer processes between them.

The heat and mass transfer processes between the nodes are numbered in figure 2 and described here:

1. Mass flow of liquid nitrous oxide out of the tank
2. Heat and mass transfer from the vapor to the liquid via condensation, diffusion, and convection
3. Heat and mass transfer from the liquid to the vapor via boiling, evaporation, diffusion, and convection
4. Heat transfer from the liquid side of the tank wall to the liquid
5. Heat transfer from the vapor side of the tank wall to the vapor
6. Heat transfer from the atmosphere to the liquid side of the tank wall
7. Heat transfer from the atmosphere to the vapor side of the tank wall

8. Heat and mass transfer from the liquid side of the tank wall to the vapor side via conduction and motion of the boundary

The dynamics of the wall nodes will be discussed later in section C and we begin here with the liquid and vapor nodes. The development presented in this section is general and is not limited to a system of two fluid nodes. To determine the number of equations needed to describe the dynamics of the liquid and vapor nodes we begin with Gibbs' Phase Rule:

$$\#\text{ degrees of freedom} = \#\text{ components} - \#\text{ phases} + 2 \tag{1}$$

This determines the number of intensive variables needed to fix the thermodynamic state of a node. An additional extensive variable is needed to fix the size of each node, expressed in any form such as mass, volume, entropy, etc. There are two additional constraints on the system. The first is from assuming that the pressure is uniform within the tank, yielding the intensive constraint

$$P_{node\ i} = P_{node\ j} \tag{2}$$

Which is actually $n-1$ constraints, where n is the number of nodes. The second constraint is extensive in nature and arises from the fixed volume of a propellant tank:

$$\sum_i V_{node\ i} = V_{tank} \tag{3}$$

Combining equations (1) through (3) we can write

$$\begin{aligned} \#\text{ equations} &= \#\text{ intensive variables} + \#\text{ extensive variables} - \text{P constraints} - \text{V constraint} \\ &= (2n_{nonsat} + n_{sat}) + n_{tot} - (n_{tot} - 1) - 1 \\ &= n_{tot} + n_{nonsat} \end{aligned} \tag{4}$$

Where n_{tot} is the total number of nodes, n_{nonsat} is the number of nodes that are not maintained at a saturation state and n_{sat} is the number of nodes that are saturated. Equation (4) dictates that at most two equations will be needed for each node in the system. The two equations of choice are conservation of mass and energy:

$$\frac{dm}{dt} = \sum(\dot{m})_{in} - \sum(\dot{m})_{out} \tag{5}$$

$$\frac{dU}{dt} = \sum\left[\dot{m}\left(h + \frac{v^2}{2} + gz\right)\right]_{in} - \sum\left[\dot{m}\left(h + \frac{v^2}{2} + gz\right)\right]_{out} + \dot{Q}_{in} + \dot{W}_{in} \tag{6}$$

In equation (6), the velocity and acceleration terms will be neglected in all the models. The pressure gradients caused by acceleration can be significant in rockets with high thrust to weight ratios, so it is possible that this assumption will create inaccuracies in flight vehicles. Equations (5) and (6) yield a system of ordinary differential equations that are integrated in time. The key features that differentiate one model from another are twofold: whether or not nodes are assumed to be saturated and the way in which the heat and mass transfer terms are modeled.

B. Outlet Flow

An important aspect of any tank model is the description of the outlet flow (arrow 1 in figure 2), which in a propulsion system is established by the injector configuration and chamber pressure. In nitrous oxide feed systems, the prediction and modeling of injectors is an ongoing research topic and there is no universally accepted method for predicting the flow rate. For this work, the model proposed by Dyer et al[8] will be used:

$$G = \frac{\kappa G_{SPI} + G_{HEM}}{1 + \kappa} \tag{7}$$

$$G_{SPI} = C_d\sqrt{2\rho_1(P_1 - P_2)} \tag{8}$$

$$G_{HEM} = C_d\rho_2\sqrt{2(h_1 - h_2)} \tag{9}$$

$$\kappa = \sqrt{\frac{P_1 - P_2}{P_{1,sat} - P_2}} \tag{10}$$

Here h_2 is found assuming that the fluid expands through the injector isentropically. Note that equation (7) in the original publication and in Whitmore & Chandler[3] had an error that was later identified by Solomon.[9] Solomon's corrected equation is shown above.

The Dyer model is a combination of the single phase incompressible (SPI) model and the homogeneous equilibrium model (HEM), each of which describes one of two regimes of the flow through an orifice. In principle, the HEM is accurate when the fluid residence time in the orifice is much longer than the bubble growth time, meaning there is sufficient time for interphase heat and mass transfer to bring the fluid to equilibrium. Conversely the SPI model is accurate when the residence time is smaller than the bubble growth time, and there is insufficient time for interphase heat and mass transfer. κ is derived as a ratio of bubble growth time to residence time in the orifice and is an indication of the dominant regime. When κ is large the Dyer model approaches the SPI model, while at low κ it approaches the HEM. For saturated liquid entering the injector, the various components of G are shown in figure 3 as a function of the downstream pressure.

Experimental work by Hesson & Peck[10] and recently by Waxman et al[11,12] has demonstrated that if the downstream pressure is significantly lower than the vapor pressure, the flow rate becomes insensitive to the downstream pressure, in contrast to equations (8) and (9). This is known as critical flow and, the Dyer flow model in general cannot predict the mass flux in this regime without making additional corrections. However, in the limited case of saturated liquid entering the injector ($P_1 = P_{1,sat}$) this type of behavior is predicted, as evidenced by the flat trajectory of the Dyer flow model in figure 3.

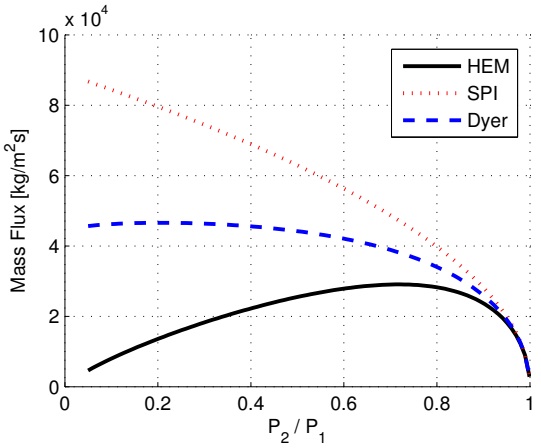

Figure 3. Predicted mass fluxes from the HEM, SPI, and Dyer models verses downstream pressure. Upstream, the conditions are saturated liquid at $293K$.

For this work, the importance of this phenomenon is that as long as the downstream pressure is appreciably below the saturation pressure, the flow rate is approximately independent of the downstream pressure and P_2 can be taken as 0 without losing accuracy. Therefore, experimental data taken in hot-fire tests and cold-flow tests can be easily used without requiring measurements of P_2. This is dependent on P_2 being significantly below $P_{1,sat}$, a condition that is violated in motors that operate at high chamber pressures but should be accurate in the data sets used throughout this work.

This result also suggests that when developing a tank model it does not need to be coupled to a combustion chamber ballistics model. Alternatively, if the combustion chamber pressure is being modeled P_2 can be inserted

In the work done by other researchers on modeling nitrous oxide tank dynamics, some (Zilliac & Karabeyoglu, Casalino & Pastrone) have chosen to use the SPI model, while others (Whitmore & Chandler) have used equation (7). In the following work only equation (7) will be used in order to provide consistency.

C. Heat Transfer and the Tank Walls

In two of the models used in this work, natural convection heat transfer is calculated. Standard correlations[13] for the Nusselt number as a function of the Rayleigh number will be used for calculating heat fluxes between the ambient air and the tank wall (arrows 6 and 7 in figure 2), between the tank wall and the propellant (arrows 4 and 5), and in the case of the Zilliac & Karabeyoglu model fluxes between the liquid free surface

and both the liquid and vapor (arrows 2 and 3). The relations used are:

$$\dot{Q} = hA\Delta T \tag{11}$$

$$h = Nu\frac{k}{L} \tag{12}$$

$$Nu = cRa^n \tag{13}$$

$$Ra = \frac{c_P \rho^2 g\beta|\Delta T|L^3}{\mu k} \tag{14}$$

Fluid properties are evaluated at the film temperature, defined as the mean of the fluid and surface temperatures. Table 1 gives values of the constants c and n used for calculations in the present work.

If heat transfer to and from the tank wall is calculated, the wall temperature must be known. Therefore, in addition to the ordinary differential equations derived from the three models in this paper, a pair of differential equations are needed to describe the tank wall temperature, both for the portion in contact with liquid and that in contact with vapor. We draw a control volume for each of the two portions of the tank wall, and applying conservation of energy to either one yields

Table 1. Heat transfer constants, from Bergman et al[13]

Fluid	Surface	c	n
Ambient air	Tank wall	0.59	1/4
Liquid N_2O	Tank wall	0.021	2/5
Vapor N_2O	Tank wall	0.021	2/5
Liquid N_2O	Saturated liquid surface	0.15	1/3
Vapor N_2O	Saturated liquid surface	0.15	1/3

$$\frac{dT_w}{dt} = \frac{\dot{Q}_{w,in} - \dot{Q}_{w,out} + \dot{Q}_{w,cond} + \dot{m}_{w,in}c_w(T_{w,in} - T_w)}{m_w c_w} \tag{15}$$

where $\dot{m}_{w,in}$ here accounts for the changing liquid level and hence the moving boundary of the control volume. The heat transfer into the wall is natural convection from ambient air, modeling a ground testing situation and not a flight vehicle. The heat transfer out of the wall is natural convection to the fluid within the tank. Conduction between the two portions of the tank wall is modeled after Corpening,[14] who approximated Fourier's heat conduction law in the following way:

$$\dot{Q}_{w,cond} = k_w A\frac{dT}{dx} \tag{16}$$

$$\frac{dT}{dx} \simeq \frac{(\Delta T)_w}{L_{w,cond}} \tag{17}$$

$$A = \pi(r_o^2 - r_i^2) \tag{18}$$

Where $L_{w,cond}$ is the distance between the center of the liquid volume and the center of the vapor volume. $(\Delta T)_w$ is the difference in temperature of the liquid and vapor sections of the wall. The result is

$$\dot{Q}_{w,cond} = \frac{k_w(\Delta T)_w\pi(r_o^2 - r_i^2)}{L_{w,cond}} \tag{19}$$

D. Numerical Methods

A difficulty in working with nitrous oxide is the calculation of thermodynamic and transport properties. Nitrous oxide's critical point (309.52 K) is near standard conditions and therefore in most systems the physical properties are sensitive to small changes in temperature or pressure. A technical equation of state has been developed for nitrous oxide by Span, Wagner, and Lemmon[15,16,17] and can be used to calculate any thermodynamic property at saturated and non-saturated states. Unfortunately no such single source exists for transport properties and instead a collection of theoretical forms fit to experimental results must be used, differing in structure for each property. The National Institute of Standards and Technology (NIST) has compiled a computer program, Refprop, that contains numerous equations of state and expressions for transport properties[18] that can be used with an extensive range of fluids. for nitrous oxide thermodynamic

properties it utilizes the technical equation of state mentioned above and for transport properties it uses a collection of sources. Refprop will be used to calculate all thermodynamic and transport properties used in this work.

A limitation of this type of technical equation of state is that they are developed by fitting theoretical functional forms to numerous sets of experimental data. While they typically are highly accurate and can often calculate $P\rho T$ properties with less than 0.5% error, their accuracy is unknown outside the range of experimental data used during development. This is problematic for modeling nitrous oxide feed systems because metastable states are often assumed to occur, requiring calculation of the properties of the fluid in these states. There is very limited data available for fluid properties in this region and hence the equation of state's accuracy is unknown. This problem was examined in a general fashion in a work by Shamsundar.[19]

An alternative to technical equations of state is to use a simpler equation of state, such as Peng-Robinson.[20] These may have reduced accuracy in general when compared to technical equations of state but are much simpler to implement and may be more accurate in the metastable region.[19] When properties are only required at saturation conditions, curve fits to experimental or EOS results can be used and have been developed by multiple groups.[4,21,22] These are typically simple functions of temperature and are the simplest to implement and use.

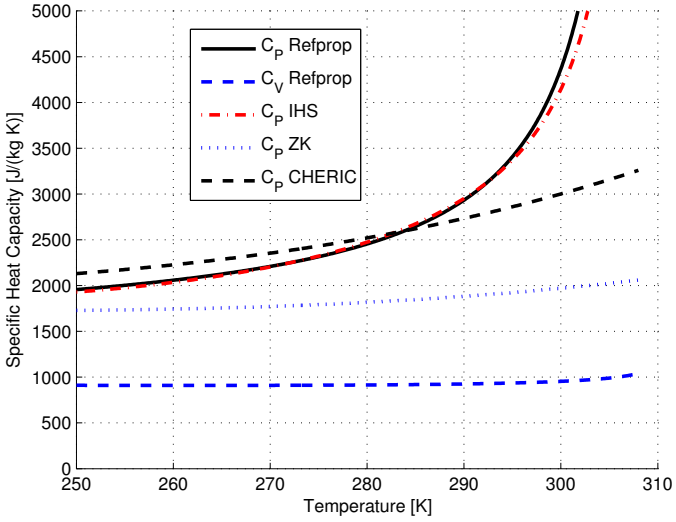

Figure 4. Specific heat capacity of saturated liquid N_2O calculated from various sources. The lines labeled IHS and CHERIC are correlations for the saturation state developed by the two organizations,[21,22] and ZK is the saturation correlation derived by Zilliac & Karabeyoglu.[4]

As a demonstration of both the sensitivity of these properties to temperature and the variability in different methods of calculating them, figure 4 shows the specific heat capacity for saturated liquid as a function of temperature. Note that different sources report values that differ by more than 100%. Also noteworthy is the large difference between the isobaric and isochoric specific heat capacity of the liquid.

All the models here are systems of ordinary differential equations and are integrated using a 4th order adaptive Runge-Kutta-Fehlberg routine.[23] This scheme was chosen over traditional 4th order Runge-Kutta methods because of its ability to calculate and control error in the results. Additionally, it poses advantages over pre-made integration routines because of the ability to manually control the step refinement near points of interest.

III. Equilibrium Model

Equilibrium models for nitrous oxide tanks have been presented by Zakirov & Li,[24] Whitmore & Chandler,[3] and Casalino & Pastrone.[5] The model presented here includes heat transfer between the fluid and the walls, which Zakirov & Li included but Whitmore & Chandler and Casalino & Pastrone did not.

The equilibrium model assumes that all propellant in the tank remains in phase equilibrium. Physically this is equivalent to assuming that the flow out of the tank is slow compared to the heat and mass transfer between the liquid and vapor. The model then consists of two saturated nodes, which (4) says requires two equations. The governing equations chosen for this model are conservation of mass and energy (equations (5) and (6)) which are applied to the combined liquid and vapor in the tank as a whole. This allows interphase heat and mass transfer calculations to be avoided. With no mass flow into the tank, only allowing flow out

via the tank outlet, and no net work done on or by the propellant, the equations simplify to

$$\frac{dm_{tot}}{dt} = -\dot{m}_{outlet} \tag{20}$$

$$\frac{dU_{tot}}{dt} = -\dot{m}_{outlet} h_{outlet} + \dot{Q}_{in} \tag{21}$$

Where $\dot{m}_{outlet}$ is calculated from equation (7) and for h_{outlet} it is assumed that saturated liquid is exiting the tank. $\dot{Q}_{in}$ is calculated from equations (11) through (14). While m_{tot} and U_{tot} are convenient variables to solve for with the simple ODE's shown above, they are not useful for determining fluid properties. The entire tank remains saturated and thus a single value of temperature or pressure would be sufficient to describe both the liquid and vapor properties. Temperature is often the more convenient variable, and so to find the fluid temperature at a given time from the variables m_{tot} and U_{tot}, the volume constraint (equation (3)) is introduced

$$V_{tank} = m_{tot}\left[\frac{1-x}{\rho_{liq}} + \frac{x}{\rho_{vap}}\right] \tag{22}$$

$$x = \frac{\frac{U_{tot}}{m_{tot}} - u_{liq}}{u_{vap} - u_{liq}} \tag{23}$$

Where ρ and u are calculated from T at saturation conditions and (23) is given for convenience and is derived from the definition of m_{tot} and U_{tot}. A value of T must be chosen such that $\rho_{liq}(T)$, $\rho_{vap}(T)$, and $x(u_{vap}(T), u_{liq}(T))$ satisfy (22). Once the temperature is known, any property of either phase can be directly computed.

We now have a set of four ordinary differential equations to integrate: (15) for $T_{w,liq}$, (15) for $T_{w,vap}$, (20) for m_{tot}, and (21) for U_{tot}. An important feature of equilibrium models is that they require properties only at the saturation state, meaning that complex equations of state are not strictly necessary. Curve fits to saturation properties such as P_{sat}, ρ_{liq}, ρ_{vap}, u_{liq}, and u_{vap} can be used in an equilibrium model in place of more complicated equations of state, simplifying and accelerating both the implementation and solution times.

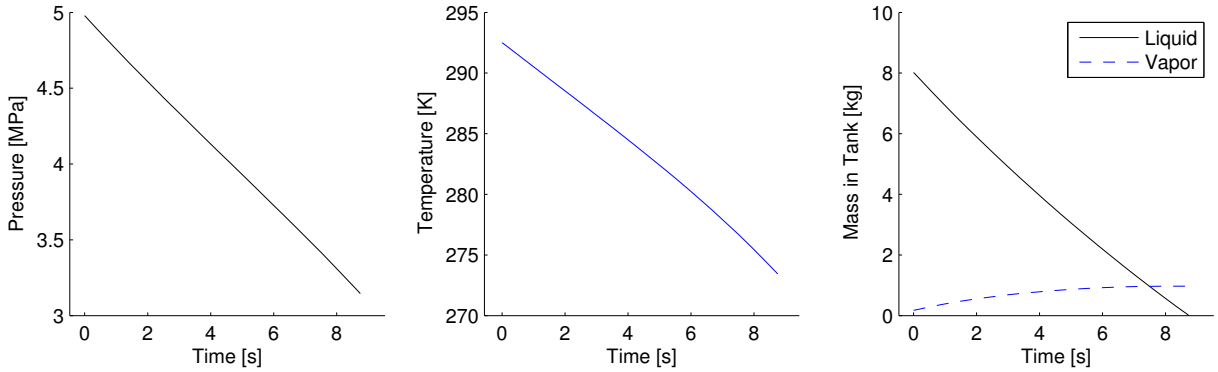

Figure 5. Pressure, temperature, and mass time histories from the equilibrium model using the conditions of Van Pelt et al.[1] Details of the conditions will be discussed later in section VI.

Figure 5 shows the results when applied to a tank typical of a small sounding rocket, namely the case of Van Pelt et al.[1] The details of this experiment will be discussed in section VI. All curves follow approximately linear trajectories, with the exception of vapor mass. Note that when compared to figure 1, the initial drop and recovery are not captured with this model. The character of these curves does not change when this model is applied with a wide variety of initial conditions.

IV. Zilliac & Karabeyoglu Model

In a paper by Zilliac & Karabeyoglu,[4] a model is presented that builds a level of complexity onto the equilibrium model by allowing the liquid and vapor to be at different temperatures and directly calculating

the heat and mass transfer between the phases. In a later work, Fernandez[25] evaluated this model in detail and also applied it to nitrous oxide tanks in which Helium pressurant was added. This type of model is based on the work of Morey & Traxler,[26] initially developed for traditional liquid propellant pressurization systems. Some alterations from the work by Zilliac & Karabeyoglu have been made but the basic assumptions and core structure of the model is retained.

Mathematically, the model contains two non-saturated nodes, which equation (4) dictates requires four equations. Therefore we apply conservation of mass and energy separately to each phase:

$$\frac{dm_{vap}}{dt} = \dot{m}_{evap} - \dot{m}_{cond} \tag{24}$$

$$\frac{dm_{liq}}{dt} = -\dot{m}_{evap} + \dot{m}_{cond} - \dot{m}_{outlet} \tag{25}$$

$$\frac{dU_{vap}}{dt} = \dot{m}_{evap}h_{evap} - \dot{m}_{cond}h_{cond} - P\frac{dV_{vap}}{dt} + \dot{Q}_{in,vap} \tag{26}$$

$$\frac{dU_{liq}}{dt} = -\dot{m}_{outlet}h_{outlet} - \dot{m}_{evap}h_{evap} + \dot{m}_{cond}h_{cond} - P\frac{dV_{liq}}{dt} + \dot{Q}_{in,liq} \tag{27}$$

The outlet flow is assumed to be from the liquid node and $\dot{m}_{outlet}$ is computed via equation (7). The heat transfer terms are now a combination of interphase processes and convection to the tank walls.

To compute the heat and mass transfer between the phases, we assume the presence of an infinitesimal layer of saturated liquid between the bulk liquid and the vapor, defined by the pressure in the tank ullage. Natural convection transports heat from the bulk liquid to this surface and also from this surface into the vapor. If the heat transfer from the bulk liquid to the surface exceeds that from the surface to the vapor, the excess is used to vaporize liquid and yields mass transfer from the liquid to the vapor. Therefore:

$$\dot{m}_{evap} = \frac{\dot{Q}_{liq\rightarrow surf} - \dot{Q}_{surf\rightarrow vap}}{\Delta h_{LV} + (h_{sat,liq} - h_{liq})} \tag{28}$$

$\dot{Q}_{liq\rightarrow surf}$ and $\dot{Q}_{surf\rightarrow vap}$ are computed via (11) through (14), however Zilliac & Karabeyoglu multiplied $\dot{Q}_{liq\rightarrow surf}$ by an empirical factor E with a value on the order of 10^3 in order to match experimental results. Therefore $\dot{Q}_{liq\rightarrow surf} = EhA\Delta T$, in contrast to equation (11). Physically, they assumed that this corrected for a heat transfer coefficient that was too low because it didn't include the effects of boiling, liquid layer motion, and blowing. Condensation is handled differently and occurs only when the pressure increases above the saturation pressure of the vapor. Then we assume that mass transfer from the vapor to the liquid occurs in the amount needed to bring the pressure to the saturation pressure in one time step:

$$\dot{m}_{cond} = \begin{cases} \dfrac{(P - P_{sat,vap})V_{vap}\mathfrak{M}_{vap}}{Z_{vap}R_{vap}T_{vap}\Delta t}, & \text{if } P > P_{sat,vap} \\ 0, & \text{if } P \leq P_{sat,vap} \end{cases} \tag{29}$$

The heat released from the condensation of this vapor is added into the vapor volume and is accounted for in the $\dot{Q}_{in,vap}$ term. Both the $\dot{Q}_{in,vap}$ and $\dot{Q}_{in,liq}$ terms also include heat transfer to/from the tank walls, which is computed via equations (11) through (14).

The work term $(P\frac{dV}{dt})$ presents a problem because $\frac{dV}{dt}$ is not explicitly known. One option is to compute it via backwards differences, but this can introduce numerical instability in some situations and therefore a different procedure is desirable. One alternative is to use the pressure and volume constraints (equations (2) and (3)) to derive an equation for $\frac{dV}{dt}$:

$$P_{vap} = P_{liq} \tag{30}$$

$$\frac{dP_{vap}}{dt} = \frac{dP_{liq}}{dt} \tag{31}$$

$$\left[\left(\frac{\partial P}{\partial T}\right)_\rho \frac{dT}{dt} + \left(\frac{\partial P}{\partial \rho}\right)_T \frac{d\rho}{dt}\right]_{vap} = \left[\left(\frac{\partial P}{\partial T}\right)_\rho \frac{dT}{dt} + \left(\frac{\partial P}{\partial \rho}\right)_T \frac{d\rho}{dt}\right]_{liq} \tag{32}$$

The thermodynamic partial derivatives $\frac{\partial P}{\partial T}$ and $\frac{\partial P}{\partial \rho}$ can be calculated from an equation of state. The time derivative of temperature can be calculated from:

$$\frac{dU}{dt} = u\frac{dm}{dt} + m\frac{du}{dt} \tag{33}$$

$$= u\frac{dm}{dt} + m\left[\left(\frac{\partial u}{\partial T}\right)_\rho \frac{dT}{dt} + \left(\frac{\partial u}{\partial \rho}\right)_T \frac{d\rho}{dt}\right] \tag{34}$$

$$\frac{dT}{dt} = \frac{1}{c_V}\left[\frac{1}{m}\left(\frac{dU}{dt} - u\frac{dm}{dt}\right) - \left(\frac{\partial u}{\partial \rho}\right)_T \frac{d\rho}{dt}\right] \tag{35}$$

And finally $\frac{d\rho}{dt}$ is found from

$$\frac{d\rho}{dt} = \frac{1}{V}\frac{dm}{dt} - \frac{m}{V^2}\frac{dV}{dt} \tag{36}$$

$$\frac{dV_{liq}}{dt} = -\frac{dV_{vap}}{dt} \tag{37}$$

A value of $\frac{dV}{dt}$ must be chosen that solves (32), entering the equation via $\frac{d\rho}{dt}$. In order to compute various properties of the two phases, the thermodynamic state of each must be specified. Given that (35) must be computed to find $\frac{dV}{dt}$, it is convenient to integrate (35) for T_{vap} and T_{liq} rather than integrating (26) and (27) for U_{vap} and U_{liq}. The internal pressure of the tank is readily chosen as the second thermodynamic state variable and can be found by using another version of the tank volume constraint,

$$V_{tank} = \frac{m_{liq}}{\rho_{liq}} + \frac{m_{vap}}{\rho_{vap}} \tag{38}$$

where $\rho_{liq} = \rho(T_{liq}, P)$ and $\rho_{vap} = \rho(T_{vap}, P)$.

The Zilliac & Karabeyoglu model is then a set of six ordinary differential equations that must be integrated: (15) for $T_{w,vap}$, and (15) for $T_{w,liq}$, (24) for m_{vap}, (25) for m_{liq}, (35) for T_{liq}, (35) for T_{vap}.

This model directly calculates the rates of heat and mass transfer between the phases and as a result at any given point in time one or both of the phases may be in a metastable state. Therefore, care is needed in calculating thermodynamic and transport properties.

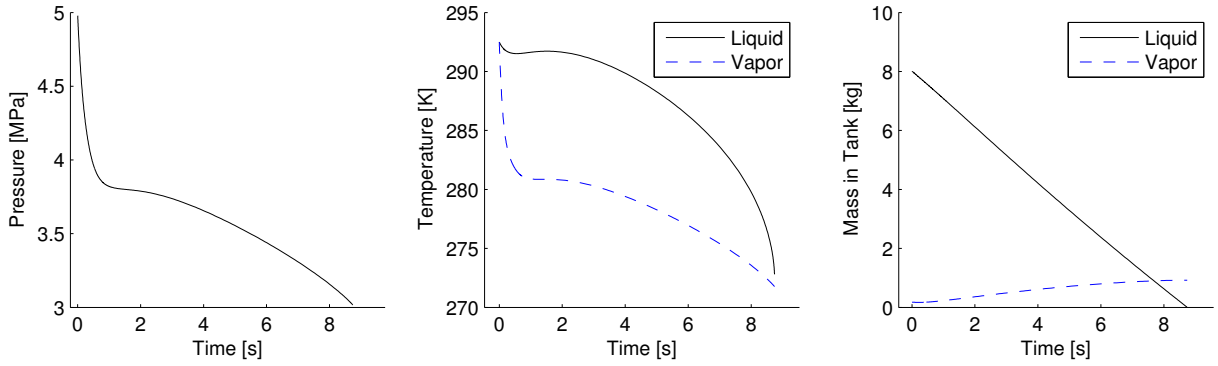

Figure 6. Pressure, temperature, and mass time histories from the equilibrium model using the conditions of Van Pelt et al.[1] Details of the conditions will be discussed later in section VI.

Figure 6 shows typical results from this model. Note that it does a much better job than the equilibrium model of capturing the non-linear nature of the pressure time history. Unlike the equilibrium model, these results do change character as experimental conditions are varied. To demonstrate one aspect of how the results change, figure 7 shows the variation seen in the pressure time history as E is varied. As E grows, it increases the amount of heat and mass transfer that occur for a given temperature difference. Therefore E can be viewed as a measure of how close the system is to an equilibrium solution. As will be shown later, E is system-dependent and is found by fitting the results of the model to experimental data.

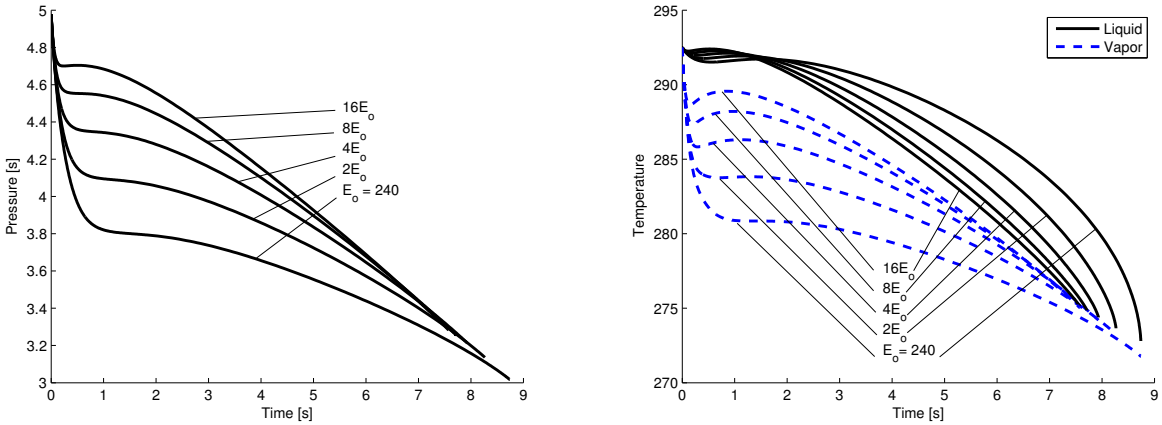

(a) Pressure

(b) Temperature

Figure 7. Pressure and temperature time histories as E is varied. The Van Pelt et al[1] case is taken as a baseline and E is increased by a factor of 16.

V. Casalino & Pastrone Model

In a paper by Casalino & Pastrone,[5] two different models for self-pressurizing propellant tank dynamics are presented. The first is an equilibrium model, and the second is what they termed a "two-phase lumped model" which will be described here. This model uses two non-saturated nodes similar to the Zilliac & Karabeyoglu model, nominally requiring four equations. However in this model a series of simplifying assumptions are made that allow for all properties to be found at the saturation state, removing the necessity for complex equations of state. The only modification made to the original model is the use of the Dyer flow model (equation (7)) in place of the SPI model (equation (8)). We begin by applying conservation of mass and energy to both the liquid and vapor nodes:

$$\frac{dm_{vap}}{dt} = \dot{m}_{evap} - \dot{m}_{cond} \tag{39}$$

$$\frac{dm_{liq}}{dt} = -\dot{m}_{evap} + \dot{m}_{cond} - \dot{m}_{outlet} \tag{40}$$

$$\frac{dU_{vap}}{dt} = \dot{m}_{evap}h_{evap} - \dot{m}_{cond}h_{cond} - P\frac{dV_{vap}}{dt} \tag{41}$$

$$\frac{dU_{liq}}{dt} = -\dot{m}_{outlet}h_{outlet} - \dot{m}_{evap}h_{evap} + \dot{m}_{cond}h_{cond} \tag{42}$$

where we've already assumed that the liquid is incompressible and there is no heat transfer between the phases or to the tank walls. By assuming that the vapor remains saturated, meaning all properties are functions only of temperature, equation (41) can be written as

$$m_{vap}\frac{du_{vap}}{dT_{vap}}\frac{dT_{vap}}{dt} - \dot{m}_{cond}\left[\Delta h_{LV}(T_{vap}) - \frac{P}{\rho_{vap}}\right] - \dot{m}_{evap}\left[h_{vap}(T_{liq}) - u_{vap}\right] = -P\frac{dV_{vap}}{dt} \tag{43}$$

Additionally we've assumed that condensing vapor leaves the ullage as saturated liquid at T_{vap} and evaporating liquid enters the ullage as saturated vapor at T_{liq}. For the liquid, if we make the idealizing assumptions that $u = h = h(T)$, equation (42) can be written as

$$c_{liq}m_{liq}\frac{dT_{liq}}{dt} = \dot{m}_{cond}\left[h_{liq}(T_{vap}) - h_{liq}(T_{liq})\right] - \dot{m}_{evap}\Delta h_{LV}(T_{liq}) \tag{44}$$

By assuming the liquid to be incompressible, the pressure constraint is no longer applicable because liquid properties are not functions of pressure. Therefore an expression different from equation (32) is needed. We

can use the volume constraint to derive:

$$\frac{dV_{vap}}{dt} = -\frac{dV_{liq}}{dt} \tag{45}$$

$$= -\frac{1}{\rho_{liq}}\frac{dm_{liq}}{dt} + \frac{m_{liq}}{\rho_{liq}^2}\frac{d\rho_{liq}}{dT_{liq}}\frac{dT_{liq}}{dt} \tag{46}$$

Note that in Casalino & Pastrone's paper where this model was presented,[5] there was a sign error in equation (46). The corrected version is shown above. In order to calculate the mass transfer from condensation and evaporation, we make some assumptions about both these processes. First, we assume that boiling does not begin until the pressure reaches a critical value, P_{lim}, which is a function of the liquid temperature and is midway between the saturation pressure and the spinodal. Before the pressure drops to this value, condensation occurs in the vapor in the amount necessary to maintain it at the saturation state. After P reaches P_{lim}, condensation ceases and then evaporation and/or boiling occurs in the amount needed to keep the pressure at P_{lim}. This is summarized as:

$$\frac{dP}{dt} = \begin{cases} \dfrac{dP_{sat}}{dT}\dfrac{dT_{vap}}{dt}, & \text{if } P > P_{lim} \\ \dfrac{dP_{lim}}{dT}\dfrac{dT_{liq}}{dt}, & \text{if } P = P_{lim} \end{cases} \tag{47}$$

Where

$$P_{lim}(T_{liq}) = \frac{1}{2}\left[P_{sat}(T_{liq}) + P_{sp}(T_{liq})\right] \tag{48}$$

$$P_{sp}(T_{liq}) = 1.98\frac{bar}{K}T_{liq} - 540bar \tag{49}$$

Where equation (49) is a curve fit developed by Casalino & Pastrone. This does not directly yield an expression for $\dot{m}_{cond}$ or $\dot{m}_{evap}$, therefore we turn to the real gas equation of state in order to relate $\frac{dP}{dt}$ to $\dot{m}$. Differentiating $PV = ZmRT$ with respect to time and rearranging gives

$$\frac{dm_{vap}}{dt} = m_{vap}\left(-\frac{1}{Z_{vap}}\frac{dZ_{vap}}{dt} - \frac{1}{T_{vap}}\frac{dT_{vap}}{dt} + \frac{1}{P}\frac{dP}{dt} + \frac{1}{V_{vap}}\frac{dV_{vap}}{dt}\right) \tag{50}$$

Which can be simplified by assuming that the vapor remains saturated

$$\frac{dZ_{vap}}{dt} = \frac{dZ_{vap}}{dT}\frac{dT_{vap}}{dt} \tag{51}$$

This value of $\frac{dm_{vap}}{dt}$ is used in equations (43) and (44) by making the substitutions:

$$\dot{m}_{cond} = \begin{cases} -\dfrac{dm_{vap}}{dt}, & \text{if } P > P_{lim} \\ 0, & \text{if } P = P_{lim} \end{cases} \tag{52}$$

$$\dot{m}_{evap} = \begin{cases} 0, & \text{if } P > P_{lim} \\ \dfrac{dm_{vap}}{dt}, & \text{if } P = P_{lim} \end{cases} \tag{53}$$

We now have a system of four ODE's to integrate: (40) for m_{liq}, (43) for T_{vap}, (44) for T_{liq}, and (50) for m_{vap}. Unfortunately, unlike the previous models the ODE's are a system of algebraic equations that must be solved simultaneously in order to calculate the derivatives. This adds some additional complexity to the implementation.

Sample results from this model are shown in figure 8. The pressure initially shows a steep drop followed by a linear decrease. This sudden change occurs when condensation ceases and boiling begins. An interesting feature is seen in the temperature history: after boiling begins, the vapor temperature increases with time, eventually exceeding its initial value. This happens because the transfer of energy into the vapor is fixed by boiling, which is in turn fixed by $P_{lim} = P_{lim}(T_{liq})$. Energy flows into the vapor during this time at a rate that is only dependent on the liquid temperature, and without regard for the vapor temperature. The basic character of these plots does not vary significantly with initial conditions.

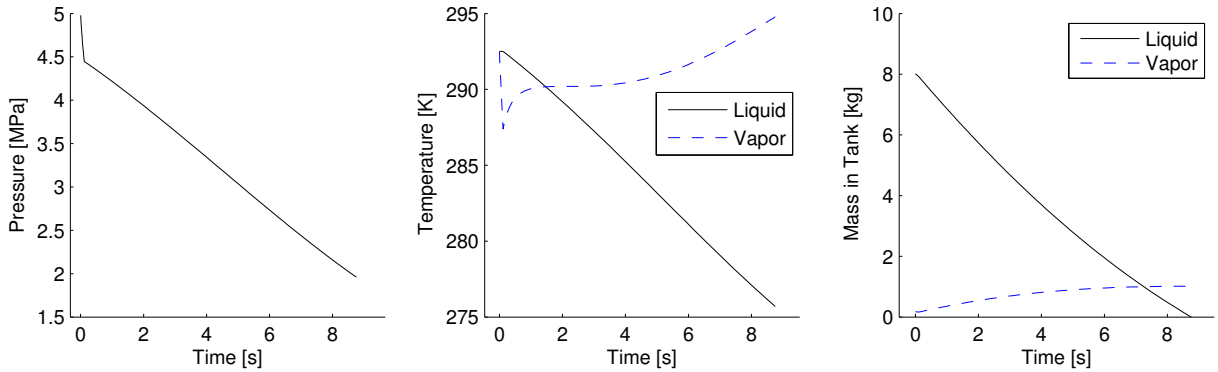

Figure 8. Pressure, temperature, and mass time histories from the equilibrium model using the conditions of Van Pelt et al.[1] Details of the conditions will be discussed later in section VI.

VI. Model Evaluation

When these models were presented by their developers, they were each compared against a different set of experimental data. It is useful to evaluate each of them against a common array of experimental data to evaluate their performance and allow for direct comparisons. Here pressure and temperature traces taken from six experiments will be given, along with the predicted traces from the three models. Additionally, one set of data includes many tests with the same system over a range of mass flow rates. This set will be used to compare how the models' predictions change as this parameter is varied.

A. Overview and Procedure

The sets of experimental data that are used in this paper are summarized here:

1. One of the blow-down cold flow tests from Zilliac & Karabeyoglu,[4] originally used to validate their model.
2. A hybrid motor firing performed by Van Pelt et al,[1] from a class project at Stanford University in 2004 that was also used as validation data for Casalino & Pastrone's model.
3. Data from ground and flight tests performed by Prince et al,[27] from a class project at Stanford University in 2013.
4. Two blow-down cold flow tests in a small scale system from a previous work by the authors.[7]

The basic features of these data sets are summarized in tables 2 and 3. The subscript i refers to the initial value and LRO to the value at the liquid run out point, where the outlet flow transitions to vapor. These four data sets represent a range of experimental conditions, and include flight data in order to see any effects of enhanced acceleration or forced convection on the tank dynamics. For convenience the models will be abbreviated as EQ, ZK, and CP, referring to equilibrium, Zilliac & Karabeyoglu, and Casalino & Pastrone, respectively.

Table 2. Tank dimensions from each data set

Data set	Volume $[m^3]$	Length $[m^3]$	Tank ID $[cm]$	Wall Thickness $[mm]$	Wall Material
Zilliac & Karabeyoglu	0.0354	1.652	19.05	3.18	Aluminum
Van Pelt et al	0.01128	1.582	9.525	3.18	Aluminum
Prince et al	$9.29 \cdot 10^{-3}$	0.813	12.07	3.18	Aluminum
Zimmerman et al	$1.80 \cdot 10^{-4}$	0.356	2.54	6.35	Polycarbonate

Table 3. Experimental conditions from each data set

Data set	Fill Level [%]	P_i $[MPa]$	T_i $[K]$	m_i $[kg]$	t_{LRO} $[s]$
Zilliac & Karabeyoglu	64	4.502	286.5	20.0	4.91
Van Pelt et al	90	4.999	292.5	8.2	8.74
Prince et al (Ground test)	95	4.777	290.7	7.2	5.56
Prince et al (Flight test)	85	5.452	296.5	6.3	4.85
Zimmerman et al (low $\dot{m}$)	87	4.091	282.7	0.14	19.88
Zimmerman et al (high $\dot{m}$)	87	3.763	278.8	0.14	4.86

The initial conditions for the models are set by the values in these tables. It is assumed that the nitrous oxide liquid and vapor begin at saturation defined by the initial pressure. In most cases this implies a temperature slightly different from the reported initial values, but since pressure measurements are frequently more accurate than temperature measurements, the pressure was chosen as more trustworthy. The initial amount of nitrous oxide in the tank, measured as m_i or fill level, is often a difficult measurement to make. Therefore we can assume that there is significant, although unquantified, uncertainty in these values in table 3. The exceptions to this are the data of Zilliac & Karabeyoglu, who used a load cell to measure the mass of propellant in the tank, and Zimmerman et al,[7] who used video imagery to locate the liquid level.

One parameter not chosen from the reported system configuration is the injector C_dA. Due to the uncertainty in modeling the flow of nitrous oxide through injectors and the variability of feed systems, instead an effective injector C_dA will be estimated. This is done by varying C_dA until the averaged mass flow rate (demonstrated by t_{LRO}) of the model matches that of the experiment. Therefore, each model uses a different C_dA for comparing to a given set of experimental data. The results are shown in table 4. Obviously this presents a problem for engineers who wish to predict performance without prior knowledge of either C_dA or t_{LRO}, but that task is outside the scope of this paper.

Table 4. Model parameters for each data set.

Data Set	C_dA $[mm^3]$			E_{opt}
	EQ	CP	ZK	ZK
Zilliac & Karabeyoglu	86.6	107	93.5	$1.3 \cdot 10^3$
Van Pelt et al	19.7	23.6	22.8	$2.4 \cdot 10^2$
Prince et al (Ground)	28.0	34.8	29.4	$5.3 \cdot 10^2$
Prince et al (Flight)	25.5	28.4	26.4	$1.0 \cdot 10^3$
Zimmerman et al (low $\dot{m}$)	0.155	0.236	0.156	$3.4 \cdot 10^2$
Zimmerman et al (high $\dot{m}$)	0.687	1.07	0.698	$7.5 \cdot 10^2$

For the ZK model, both E and C_dA affect t_{LRO} so the process is more complicated. The values of E and C_dA were chosen to minimize the integrated deviation between the modeled pressure history and the experimental pressure history, shown in equation (54). The denominator in this relation is included for normalization. This is of course still subject to the constraint that t_{LRO} is equal to the experimental value. The values of E determined in this way (designated E_{opt}) vary from 240 to 1300 and do not appear to be correlated with any parameters of the system. There are even large differences between two tests with the

same system, indicating that it is not merely a function of tank dimensions.

$$P_{error} = \frac{\int_0^{LRO} |P_{model} - P_{exp}| dt}{\int_0^{LRO} P_{exp}\, dt} \tag{54}$$

B. Evaluation of Time Histories

We begin by comparing each model to the data of Zilliac & Karabeyoglu.[4] In figure 9, the three models are compared against the experimental pressure time history. The ZK model clearly outperforms either the EQ or CP models, with each respectively over- and under-predicting the pressure. This is consistent with the variation in C_dA in table 4, where the CP model has a larger value to compensate for the lower pressure and the EQ model has a higher value. The EQ model does reproduce the slope of the pressure trace in the linear region after $t = 2s$, and the CP model is fairly accurate before the linear region begins.

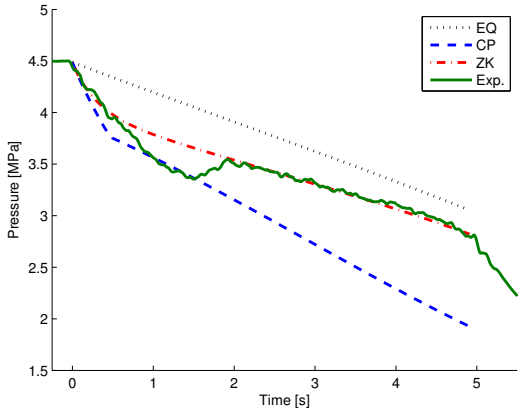

Figure 9. Comparison of model results to the experimental data of Zilliac & Karabeyoglu.[4]

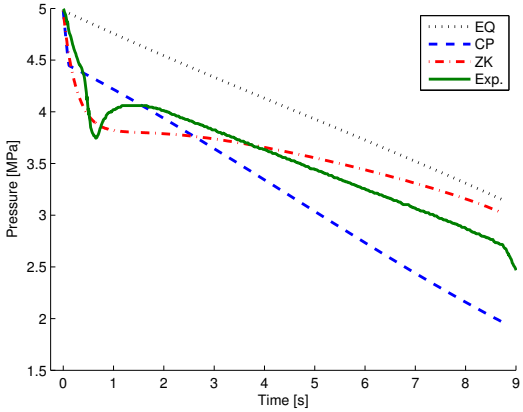

Figure 10. Comparison of model results to the experimental data of Van Pelt et al.[1]

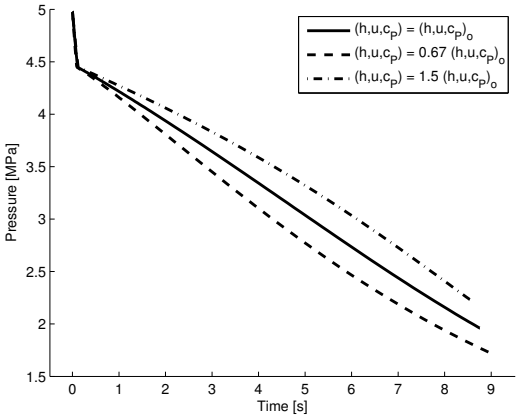

Figure 11. Pressure time histories from the CP model, showing effects of varying thermodynamic properties. Results are shown for the nominal values of h, u, c_P and also when they are multiplied by 1.5 and 0.67.

Next we compare the models to the pressure data of Van Pelt et al[1] in figure 10. Physically this data set utilized a tank that was about one third the size of the previous experiment by Zilliac & Karabeyoglu. None of the models do particularly well here, although the ZK model does the best of the three. Again, the EQ model reproduces the slope of the linear region well.

In Casalino & Pastrone's paper they showed better results when comparing their model to these data, possibly because they used a different source for nitrous oxide physical properties. In equation (44) the rate of change of liquid temperature is scaled by the liquid specific heat capacity, which was shown in figure 4 to have significant variation depending on the source of the data. Furthermore, most of the time is spent in the boiling/evaporation region, where the tank pressure is dictated by the liquid temperature.

As a demonstration of this effect, figure 11 shows the pressure traces generated by the CP model as the thermodynamic variables h, u, and c_P are scaled. The variation in pressure that results is significant, increasing or decreasing the value by up to 0.5 MPa. The variation in thermodynamic properties needed to produce this change in results is well within the range seen in figure 4.

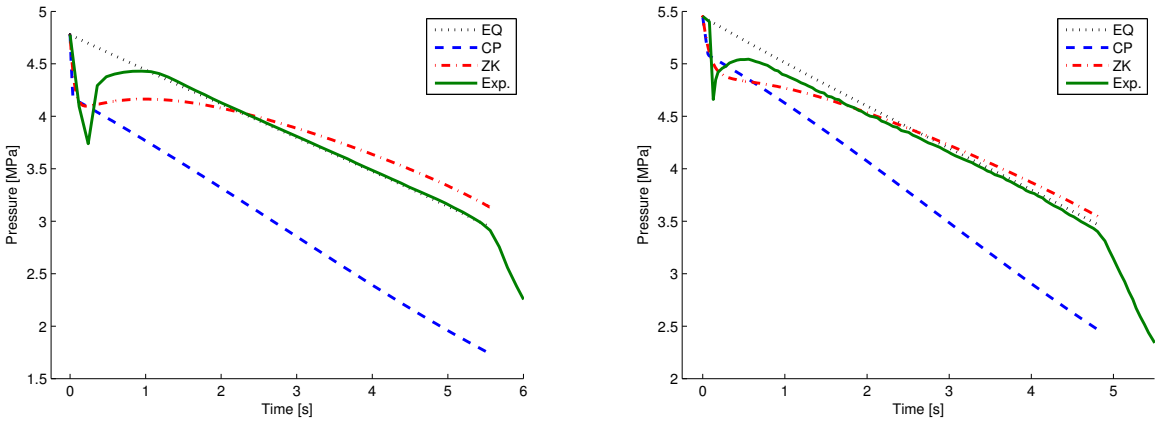

(a) Ground (b) Flight

Figure 12. Comparison of model results to the ground and flight test data of Prince et al.[27]

Now we compare to the ground and flight test data of Prince et al in figure 12. The size of this system is similar to the previous test of Van Pelt et al. In this case, with the exception of the initial drop and recovery the EQ model predicts the pressure history quite well for both the ground and flight test. The ZK model also does relatively well, with better accuracy than EQ during the initial transient and worse performance in the linear region. The CP model performs poorly here and under-predicts the pressure for the extent of the tests. The similarity between the ground and flight experimental data suggests that the effects of acceleration on the fluid and forced air convection on the tank walls are not significant. This result suggests both test data and tank models used in ground testing can be used for flight without loss of accuracy.

It is worthy of note that in figure 12 the experimental data were only sampled at about 15 Hz. Given the short time scale of the initial drop and recovery seen in self-pressurizing propellant tanks, it's possible that some features were not accurately captured in this region.

An earlier work by the authors[7] is convenient to use as a test case because numerous experiments were performed with the same system over a range of mass flow rates (ie t_{LRO} or C_dA). Here we chose two tests to examine, one at a high flow rate and one at a low flow rate. The system used in these tests is much smaller than those in the data sets mentioned previously, holding only $140g$ of nitrous oxide. The initial temperature was also lower, causing the initial pressure to be lower as well. This system was equipped with a thermocouple positioned in the outlet flow from the tank, upstream of the "injector," and gave a measure of the temperature of the effluent, taken here to be equal to the temperature of the liquid in the tank. The low mass flow rate data are shown in figure 13, and the high mass flow rate data are shown in figure 14.

Beginning with the low mass flow rate data, the pressure is predicted best by the ZK model although the overall slope is incorrect. The EQ model does somewhat worse, under-predicting the pressure for more than half of the time span. The CP model significantly under-predicts the pressure here. One possible reason for the CP model's deficiency is the linear fit for the spinodal pressure, equation (49). It is unknown how accurate this fit is and over what temperature range it is appropriate. The tests in the small scale system had significantly lower initial liquid temperatures when compared to the other tests and this corresponds to a much lower spinodal pressure predicted by equation (49).

The CP model, unlike the EQ and ZK models, assumes an adiabatic tank. This could be a second possible cause for the CP model's inaccuracy in the Zimmerman et al tests because at small size scales the ratio of surface area to volume increases, and therefore heat transfer through the tank walls may be a more significant effect than in the larger tanks. This can be evaluated by looking at the ratio of the heat transfer rate from the wall into the liquid to the liquid mass, $\dot{Q}/m_{liq}$. This ratio is proportional to the increase of the liquid temperature caused by heat transfer from the wall. In figure 15, this ratio is plotted versus time

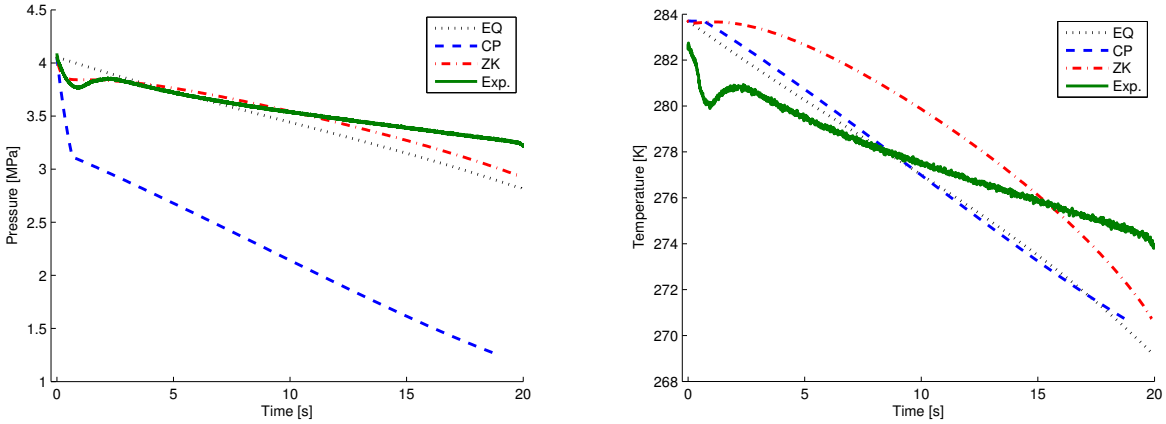

(a) Pressure (b) Temperature

Figure 13. Comparison of experimental pressure and temperature to the results of models. Data are from the low flow rate test data of Zimmerman et al.[7]

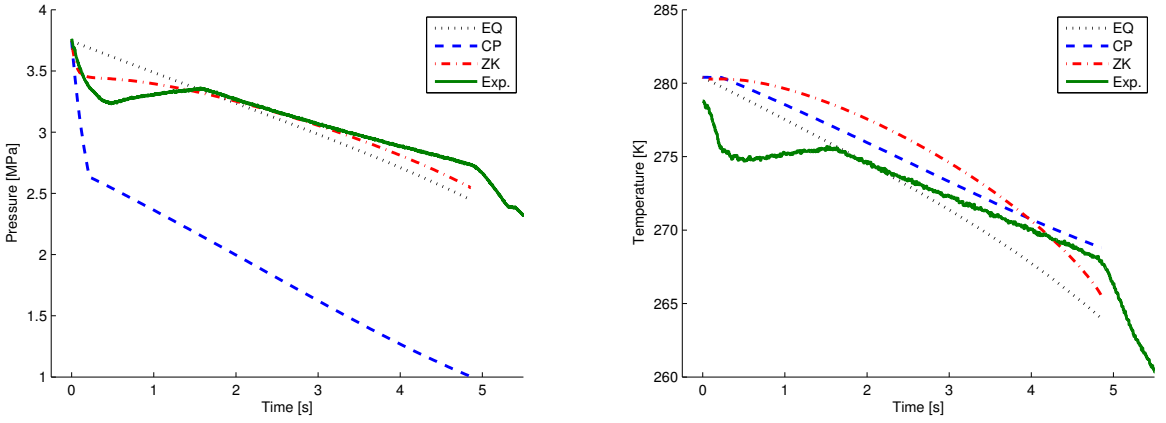

(a) Pressure (b) Temperature

Figure 14. Comparison experimental pressure and temperature to the results of models. Data are from the high flow rate test data of Zimmerman et al.[7]

for two cases, the high mass flow rate test of Zimmerman et al and the test of Zilliac & Karabeyoglu. The Zilliac & Karabeyoglu test clearly shows a much larger value, indicating that in the Zimmerman et al test the wall heat transfer term is not as important than in the Zilliac & Karabeyoglu test. We can therefore conclude that the assumption in the CP model of an adiabatic tank is not a likely cause of its inaccuracy here. This is a result of the thick polycarbonate tank wall, which with its very low thermal conductivity is a good insulator.

The temperature traces shown in figure 13 show that no model predicts the temperature with any accuracy. Not only is the overall slope of all the models much too low, none come close to predicting the initial transient which is similar in shape to that seen in the pressure time history. The ZK model in particular shows significant curvature that is not present in the experimental data. This has serious implications for the calculation of mass flow rate because the liquid density is sensitive to temperature in the regions encountered in these systems.

In figure 14 the pressure and temperature data are shown from the high mass flow rate test. The ZK model does a good job of reproducing the pressure here, although it does not fully capture the initial transient. The EQ model also performs reasonably well although it under-predicts the pressure during the linear region. The CP model fairs poorly and significantly under-predicts the pressure.

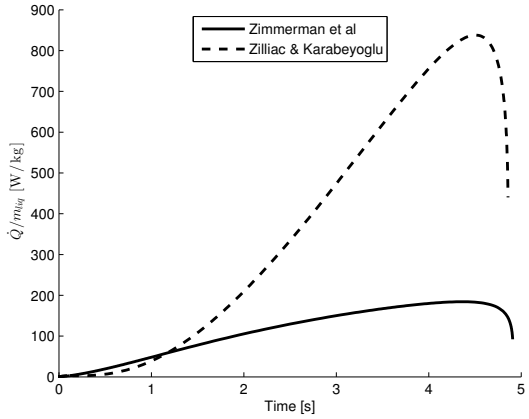

Figure 15. Specific heat transfer rate from tank wall into liquid, as predicted from ZK model. Results shown for the high mass flow rate test of Zimmerman et al and for the blow-down test of Zilliac & Karabeyoglu.

The models do a slightly better job of reproducing the temperature history for this test than they did for the low flow rate test. After the initial transient the CP model captures the linear portion of the temperature profile quite well. The EQ model predicts a temperature drop that is faster than the experimental data, while the ZK model fairs poorly.

The results here can be discussed quantitatively by calculating the error in predicted pressure history (equation (54)) for each of the three models and each of the six experimental data sets. This is done in table 5. Of the three models, the ZK model performs the best, with errors consistently less than 5%. The EQ model is next, with errors under 15% for all cases, and as low as 1.69% for one test. The CP model performs the worst, with errors ranging from 9.68% to 39.5%. Again, this could be a result of using a different source for thermodynamic properties than what Casalino & Pastrone used in developing the model.

An important issue for those who wish to use the ZK model without prior measurements of E is the sensitivity of P_{error} to E. To that end, a modeling test was performed on the six experiments used in this work: E was fixed to the average of the six E_{opt} ($E_{ave} = 693$) and then C_dA was solved for again in order to match the experimental t_{LRO}. The pressure histories were recomputed and the resulting errors as calculated by equation (54) for each case are listed in table 5. In most cases errors only increased slightly, but for the data of Van Pelt et al, it increased to 9.69%, making it slightly less accurate than the CP model. Note that in figures 9 through 14 E_{opt} was used rather than E_{ave}.

C. Evaluation of Parameter Variations

These figures are useful in evaluating the general predictive ability of the three models for a given oxidizer feed system. Another test of the models is possible by looking at how the results change as parameters are varied. In other words, instead of looking at the pressure time history that a given model predicts, it is also useful to look at how the pressure trace changes when initial conditions change. The experiments of Zimmerman et al[7] allow for this comparison because many tests were done with the same experimental setup at a range of mass flow rates.

To evaluate the models, two quantities are evaluated: P_{LRO}/P_i and T_{LRO}/T_i. These are the pressure and temperature at the end of the liquid portion of the test, normalized by their initial values. They are plotted in figures 16 and 17 as a function of $1/t_{LRO}$ which is effectively the average mass flow rate because

Table 5. Normalized error in pressure histories, calculated via equation (54). Values are in percent.

Data Set	Pressure Error, %				Model with Minimum Error
	EQ	CP	ZK, E_{opt}	ZK, E_{ave}	
Zilliac & Karabeyoglu	10.8	12.2	1.91	2.67	Zilliac & Karabeyoglu
Van Pelt et al	14.6	9.68	4.61	9.69	ZK when $E = E_{opt}$, CP when $E = E_{ave}$
Prince et al (Ground)	1.69	21.7	3.63	3.70	Equilibrium
Prince et al (Flight)	2.44	11.9	1.99	2.38	Zilliac & Karabeyoglu
Zimmerman et al (low $\dot{m}$)	4.27	34.9	2.21	2.86	Zilliac & Karabeyoglu
Zimmerman et al (high $\dot{m}$)	4.66	39.5	1.97	2.00	Zilliac & Karabeyoglu

each test began with the same mass of nitrous oxide. Also shown in these figures are the experimental results of Zimmerman et al.[7]

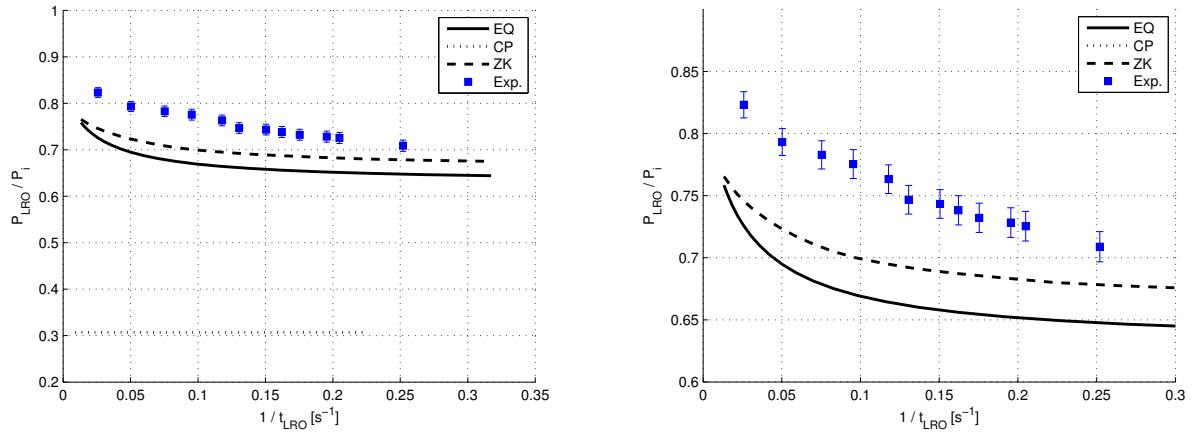

(a) All data

(b) Zoomed to region near experimental data

Figure 16. Normalized pressure at the liquid run out point as a function of $1/t_{LRO}$. Shown are the results of the three models and the experimental findings from Zimmerman et al.[7]

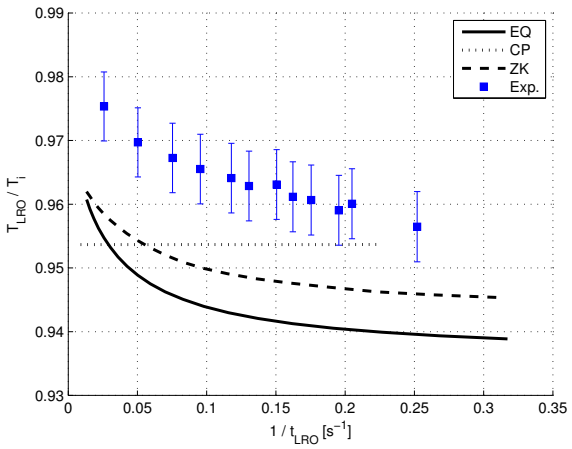

Figure 17. Normalized temperature at the liquid run out point as a function of $1/t_{LRO}$. Shown are the results of the three models and the experimental findings from Zimmerman et al.[7]

There are several implications of these results. First, the CP model in both the pressure (figure 16) and temperature (figure 17) plots is constant as t_{LRO} changes. This means that the CP model results are not dependent on the test time scale, and one set of results can be remapped to another set with a different t_{LRO} (and hence C_dA) by simply stretching or compressing the time axis.

Physically, these constant values imply that in the development of the CP model we've assumed that processes within the tank are much faster than the rate at which mass is removed via the tank outlet. The key part of the model where this takes place is described by equation (47). This states that initially, condensation occurs at *the rate required to maintain the vapor at saturation.* Then, once the limit pressure is

reached, boiling occurs at *the rate required to keep the pressure at the limit pressure*. In other words, boiling and condensation are occuring at a time scale much smaller than that of mass exiting the tank and the processes are unaffected by the change in flow rate.

The EQ model makes a similar assumption by stating that all propellant in the tank is at a uniform temperature and remains in phase equilibrium. However, the inclusion of heat transfer from the tank walls creates a dependence on mass flow rate and therefore it shows different values of P_{LRO}/P_i and T_{LRO}/T_i as the flow rate changes. In essence, as t_{LRO} drops there is less time for heat to flow into the nitrous oxide from the walls.

Figures 16 and 17 also show us that the EQ model and ZK model both predict the trend in pressure and temperature variations as mass flow rate changes, but under-predict both values. Additionally, they seem to show more curvature at low mass flow rates than the experimental data. The ZK model is closer in value to the experimental data than the EQ model. The CP model gives pressures that are much lower than seen in the experiments, consistent with the pressure time history plots of this system (figures 13 and 14).

VII. Conclusions

To summarize, this paper has taken three models (equilibrium, Casalino & Pastrone, and Zilliac & Karabeyoglu) for self pressurizing propellant tank dynamics and compared them to a wide variety of experimental data. This was done with the goal of identifying the relative advantages and disadvantages of each of the models and developing guidelines for when to use each of them. The key results for each model can be listed as:

Equilibrum Model The equilibrium model is by far the easiest to implement and solve, with the simplest differential equations and requiring properties only at saturation. Sometimes it accurately predicts the pressure time history, and other times it gives values higher than experimental data show. It cannot capture the initial transient. It does not accurately produce temperature time histories, at least when compared to the small-scale data of Zimmerman et al. It does predict the variation in P_{LRO} and T_{LRO} fairly well as t_{LRO} changes, although it's values are offset from experimental results.

Zilliac & Karabeyoglu Model This model is the hardest to implement and requires an equation of state in order to calculate properties away from saturation. Solution times are also the longest of the three models. Its accuracy at reproducing experimental pressure traces is the most consistent out of the three models, but requires determination of E. Values for this parameter range from 240 to 1300 and have no known relationship to experimental parameters. An average value of $E = 693$ was shown to give good results in most cases. The ZK model does not predict temperature profiles well, but does a good job of estimating the changes in P_{LRO} and T_{LRO} as t_{LRO} changes.

Casalino & Pastrone Model In terms of implementation and solution, the CP model is a compromise between the EQ and ZK models. It has more complex differential equations than the EQ model, but only needs properties at saturation and hence does not require a full equation of state. When compared to the experimental data used in this paper, the CP model did not do a particularly good job of accurately reproducing either pressure or temperature. It is possible that the original authors used a different source for fluid properties which could have a significant impact on the results. A key physical assumption in the model makes its results functionally independent of t_{LRO} except for a scale factor, so it cannot predict the changes that occur as t_{LRO} varies. On the other hand, this allows a single set of results to be used for many different values of t_{LRO}, simplifying design studies.

Based on these results, the ZK model is recommended when there is prior knowledge of the value of the empirical factor E, and computational effort and complex implementation are acceptable in return for increased accuracy. In all other situations, the EQ model is recommended. Ultimately though in many cases the accuracy of these models both in calculating pressure and temperature is unacceptable for practical design purposes. This work underscores the need for a robust and accurate tank model that can be used in a wide variety of systems to accurately predict experimental results.

Acknowledgments

The authors would like to thank NASA's Office of the Chief Technologist for funding this work under Space Technology Research Fellowship #NNX11AN14H and FAA's Office of Commercial Space Transportation for additional funding. This work was also supported in part by a National Defense Science and Engineering Graduate Fellowship. We would like to thank Jeremy Corpening of Teledyne Brown Engineering and Harry Ryan of NASA Stennis Space Center for their valuable assistance.

References

[1]Pelt, D. V., Hopkins, J., Skinner, M., Buchanan, A., Gulman, R., Chan, H., Karabeyoglu, M. A., and Cantwell, B. J., "Overview of a 4-inch OD Paraffin-Based Hybrid Sounding Rocket Program," *40th AIAA/ASME/SAE/ASEE Joint Propulsion Conference and Exhibit*, No. July, Fort Lauderdale, FL, 2004, pp. 1–27.

[2]Karabeyoglu, A., Dyer, J., Stevens, J., and Cantwell, B., "Modeling of N2O Decomposition Events," *44th AIAA/ASME/SAE/ASEE Joint Propulsion Conference & Exhibit*, Hartford, Connecticut, 2008, pp. 1–29.

[3]Whitmore, S. A. and Chandler, S. N., "Engineering Model for Self-Pressurizing Saturated-N2O-Propellant Feed Systems," *Journal of Propulsion and Power*, Vol. 26, No. 4, July 2010, pp. 706–714.

[4]Zilliac, G. and Karabeyoglu, M. A., "Modeling of Propellant Tank Pressurization," *41st AIAA/ASME/SAE/ASEE Joint Propulsion Conference & Exhibit*, Tucson, Arizona, 2005, pp. 1–25.

[5]Casalino, L. and Pastrone, D., "Optimal Design of Hybrid Rocket Motors for Microgravity Platform," *Journal of Propulsion and Power*, Vol. 24, No. 3, May 2008, pp. 491–498.

[6]Zimmerman, J. E., Cantwell, B., and Zilliac, G., "Initial Experimental Investigations of Self-Pressurizing Propellant Dynamics," *48th AIAA/ASME/SAE/ASEE Joint Propulsion Conference & Exhibit*, No. August, Atlanta, Georgia, 2012, pp. 1–23.

[7]Zimmerman, J. E., Waxman, B. S., Cantwell, B. J., and Zilliac, G. G., "Comparison of Nitrous Oxide and Carbon Dioxide with Applications to Self-Pressurizing Propellant Tank Expulsion Dynamics," *60th JANNAF Propulsion Meeting*, Colorado Springs, CO, 2013, pp. 1–22, available by contacting jonahz@stanford.edu.

[8]Dyer, J., Doran, E., Dunn, Z., and Lohner, K., "Modeling Feed System Flow Physics for Self-Pressurizing Propellants," *43rd AIAA/ASME/SAE/ASEE Joint Propulsion Conference & Exhibit*, No. July, Cincinnati, Ohio, 2007, pp. 1–13.

[9]Solomon, B. J., *Engineering Model to Calculate Mass Flow Rate of a Two-Phase Saturated Fluid Through an Injector Orifice*, Ph.D. thesis, Utah State University, 2011.

[10]Hesson, J. C. and Peck, R. E., "Flow of Two-phase Carbon Dioxide Through Orifices," *AIChE Journal*, Vol. 4, No. 2, 1958, pp. 207–210.

[11]Waxman, B. S., Zimmerman, J. E., Cantwell, B. J., and Zilliac, G. G., "Mass Flow Rate Characterization of Injectors for Use with Self-Pressurizing Oxidizers in Hybrid Rockets," *60th JANNAF Propulsion Meeting*, 2013.

[12]Waxman, B. S., Zimmerman, J. E., Cantwell, B. J., and Zilliac, G. G., "Mass Flow Rate and Isolation Characteristics of Injectors for Use with Self-Pressurizing Oxidizers in Hybrid Rockets," *49th AIAA/ASME/SAE/ASEE Joint Propulsion Conference and Exhibit*, AIAA, San Jose, CA, 2013, pp. 1–32.

[13]Bergman, T., Incropera, F., Lavine, A., and DeWitt, D., *Fundamentals of Heat and Mass Transfer*, John Wiley & Sons, seventh ed., 2011.

[14]Corpening, J. H., "Analytic Modeling of Pressurization and Cryogenic Propellant Conditions for Lunar Landing Vehicle," *57th JPM / 7th Modeling and Simulation / 5th Liquid Propulsion / 4th Spacecraft Propulsion Joint Subcommittee Meeting, Colorado Springs, CO*, 2010.

[15]Span, R. and Wagner, W., "Equations of state for technical applications. I. Simultaneously optimized functional forms for nonpolar and polar fluids," *International journal of thermophysics*, Vol. 24, No. 1, 2003, pp. 1–39.

[16]Span, R. and Wagner, W., "Equations of State for Technical Applications . III . Results for Polar Fluids," *International Journal*, Vol. 24, No. 1, 2003.

[17]Lemmon, E. W. and Span, R., "Correlations Short Fundamental Equations of State for 20 Industrial Fluids," *Journal of Chemical and Engineering Data*, Vol. 51, No. 3, 2006, pp. 785–850.

[18]Lemmon, E., Huber, M., and McLinden, M., "NIST Standard Reference Database 23: Reference Fluid Thermodynamic and Transport Properties (REFPROP), Version 9.0," 2010.

[19]Shamsundar, N. and Lienhard, J., "Equations of state and spinodal lines a review," *Nuclear Engineering and Design*, Vol. 141, No. 1-2, June 1993, pp. 269–287.

[20]Peng, D.-Y. and Robinson, D. B., "A New Two-Constant Equation of State," *Industrial & Engineering Chemistry Fundamentals*, Vol. 15, No. 1, Feb. 1976, pp. 59–64.

[21]Walter, G. H., "Thermophysical properties of nitrous oxide," Tech. Rep. September, IHS ESDU, 1991.

[22]Lee, C. S., Yoo, K.-P., Kim, W. Y., and Lee, H., "Korea Thermophysical Properties Data Bank: Properties of Pure Nitrous Oxide," Tech. rep., Chemical Engineering Research Information Center.

[23]Fehlberg, E., "Low-order classical Runge-Kutta formulas with stepsize control and their application to some heat transfer problems," Tech. Rep. July, NASA (TR R-315), Washington, D.C., 1969.

[24]Zakirov, V. A. and Li, L., "1-D , Homogeneous Liquefied Gas Self-Pressurization Model," *European Conference for Aerospace Sciences (EUCASS)*, AAAF/RAs/ASBC, Moscow, Russia, 2005, pp. 1–7.

[25]Fernandez, M., *Propellant tank pressurization modeling for a hybrid rocket*, Ph.D. thesis, 2009.

[26]Morey, T. F. and Traxler, J. J., "Pressurizing Gas Thermodynamics," *Rocket Propellant and Pressurization Systems*, edited by E. Ring, chap. 18, Prentice-Hall, Inc., Englewood Cliffs, New Jersey, 1964, pp. 211–245.

[27]Prince, E. R., Krishnamoorth, S., Ravlich, I., Kotine, A., Fickes, A. C., Fidalgo, A. I., Freeman, K., Anderson, K., and Gerson, D., "Design, Analysis, Fabrication, Ground-Test and Flight of a Two-Stage Hybrid and Solid Rocket," *49th AIAA/ASME/SAE/ASEE Joint Propulsion Conference and Exhibit*, AIAA, San Jose, CA, 2013.